Tunable Filters for Agile 5G New Radio Base Transceiver Stations [Application Notes]

Tunable Filters for Agile 5G New Radio Base Transceiver Stations

Authors: E. Doumanis, G. Goussetis, J. Vuorio, K. Hautio, O. Amper, E. Kuusmik, J. Pallonen

Efstratios Doumanis, RF/Antenna research engineer, Nokia Bell Labs, Espoo, Finland, Efstratios.doumanis@nokia.com

Prof. George Goussetis, Professor of microwave & antenna Engineering, Heriot Watt University, Edinburgh, UK, g.goussetis@hw.ac.uk

Jaakko Vuorio, Mechanical research engineer, Nokia, Espoo, Finland, Jaakko.vuorio@nokia.com

Kari Hautio, Electronic research engineer, Nokia, Espoo, Finland, kari.hautio@nokia.com

Oskari Amper, Mechanical research engineer, Nokia Bell Labs, Espoo, Finland, Oskari.amper@nokia.com

Eduard Kuusmik, Research Manager, Nokia, Espoo, Finland, eduard.kuusmik@nokia.com

Jorma Pallonen, Research Manager, Nokia Bell Labs, Espoo, Finland, Jorma.pallonen@nokia.com

Introduction:

Driven by spectrum scarcity and pressures to reduce costs, the complexity of the wireless environment is continuously growing. The need for flexible radio systems that enable efficient spectrum utilization is becoming increasingly urgent in order to optimize the use of spectrum and telecommunication infrastructure [1]-[9]. In cellular systems, the requirement for agile RF front-ends is driven by the evolution of standardization and associated spectrum and channel allocations. The evolution from 4G to 5G and beyond is marked by increased spectrum allocation to these systems both in the sub-6 GHz (FR1) and mm-wave (FR2) ranges and a multiplicity of frequency bands of operation. Underpinning cellular infrastructure that can serve a number of frequency bands utilizing common hardware therefore delivers operational and commercial advantages.

Agile RF front-ends remain the major remaining technological bottleneck in the pathway to exploiting the full benefits of software defined radio technology in cellular Base Transceiver Stations (BTSs). In the future, such systems could dynamically adjust radio access in order to optimise network capacity and traffic service in light of the wireless spectrum scarcity. The availability of frequency agile radios would further enable accommodating for the multiplicity and evolution of cellular standards at minimum cost, since a BTS installation could be reconfigured to serve multiple existing and emerging standards and bands. This can be particularly beneficial in light of the trend towards ever smaller cells and remote radio heads (RRHs), which reflects to a higher number of more difficult-to-access accessible radio deployments. Concurrently this trend calls for minimising the radio unit volume and mass budget, which is particularly critical for sub-6 GHz bands. This is

markedly the case in urban areas, where the space for wireless service providers to install their base stations is very limited due to expensive real estate and/or loading constraints on certain installation locations such as light poles or power lines.

The needs of network operators, in turn, are major drivers to infrastructure providers who are thus striving to develop high-performing, compact and low-cost agile front-end technologies. Beyond meeting the customers' needs, agility can further have significant impact on production cost for manufacturers supplying a global market; it enables manufacturing of reduced number of standard units at larger volumes, which have the capability to cover multiple systems and can be easily reconfigured during or post deployment to fit the required frequency plans. In this respect radio agility can further reduce the delivery timescales, which has a become a key factor for the deployment of wireless systems, as manufacturers can stock and ship products on demand.

Reconfigurable microwave filters in 5G Base Transceiver Stations

Microwave filters are critical elements serving a variety of functions in BTS radio front-ends. In receive chains, filters are deployed to suppress interfering signals, limit the received noise as well as relax the phase noise and dynamic range requirements. In transmit chains, filters are commonly used to suppress the signals generated from non-linear mixing and amplification stages. Other filter applications include channel selection in radio transponders of terrestrial and satellite systems. The electrical and mechanical requirements are strongly linked with the operational scenario. Transmit filters typically call for increased power levels and high quality factors. Particularly for lower frequencies, these features often lead to heavy, bulky and costly solutions. Transmit filters operating at frequencies below 6 GHz therefore present among the most stringent challenges and hence are the focus of this paper. Enabling tunable response for these components is a major milestone towards agile RF front-ends.

In BTSs, transmit filters play a central role in the suppression of unwanted emissions. Standardisation bodies distinguish unwanted emissions into *out-of-band emissions* and *spurious emissions* [3GPP] [10]. The former occur immediately outside the channel bandwidth and are attributed to the modulation process and the spectral regrowth occurring at the power amplification stage. The latter are associated with emission of harmonic signals other intermodulation and frequency conversion products or parasitic emission. Suppressing both out-of-band and spurious emissions pose requirements for steep roll-off selectivity as well as far out of band rejection. Coupled with the requirements for high power handling as well as low and stable in-band insertion loss, transmit filter implementations typically rely on high-Q resonators.

Figure *1* shows a generic simplified system block diagram of a BTS. The architecture involves the 4G/5G digital baseband processor, the ADC and DAC converters, the wideband power amplifier (Tx) and wideband LNA (Rx) followed by the filtering stage. The generic simplified block diagram of a multi-band BTS architecture deploying existing technologies with fixed response for the filtering stage is shown in Figure *1*a. It comprises a filter bank coupled with a switch matrix, which ensures the signal is forwarded to the appropriate frequency path. When it comes to spectrum agility, this approach provides a mature solution at a cost of significant redundancies and associated penalties in the size and architectural complexity. The availability of tunable filter technology would instead enable to replace the filtering stage with the layout presented in Figure *1*b. Here the filter stage adapts to the desired frequency band by virtue of tuning the centre frequency of the filters.

As evident in the schematics of Figure *1*, tunable filters bring savings not only in terms of the filter bank reduction but also in terms of eliminating the need for a switch matrix. Trade-off considerations between the filter bank and tunable filter solutions should thus be made in light of aforementioned savings. For example, in terms of signal attenuation the filter bank implementation involves additional insertion loss penalties associated with two stages of switches. Moreover, physical volume constraints may lead to volume limitations per filter to all the filters in a bank, which may lead to additional insertion loss associated with miniaturisation penalties. This is particularly relevant for radios accommodating for a large number of frequency bands, compact radios on the mast and/or radios serving in the sub 1 GHz range. Additional advantages of the tunable filter BTS may rise from savings in system complexity and costs.

Despite aforementioned system level advantages, implementing tunable filters capable and flexible enough to replace the current state-of-the-art fixed frequency equivalents has proven to be quite a formidable task [2]. The fixed filters that are currently used in multi-band cellular BTS and satellite applications have very stringent requirements and any tunable filters used to replace such filters must meet the same stringent requirements [2] across the operating range. There is a number of technical challenges linked with this that include, but are not limited to electrical requirements (e.g. achieving a wide tuning range, maintaining high-Q over a wide tuning range, maintaining a constant bandwidth), mechanical requirements (e.g. minimizing the complexity of the tuning mechanism and integrating the mechanical solution into a compact filter unit to minimize the volume, weight and power consumption) while maintaining a low cost.

Focusing on the frequency range below 1 GHz, a tuning range of the centre frequency of at least 200 MHz is required to cover the vast majority of currently specified 4G and 5G bands. For example, a tuning range of 205

MHz is required for a tunable filter that covers the bands between the 5G New Radio n12 band (centre frequency 737.5 MHz) and the n8 band (centre frequency 942.5 MHz) [10]. This range, which corresponds to fractional value approximating 25%, includes seven out of eight sub-1GHz 4G/5G bands offering both up- and down-link (with the exception of the n71 US digital band). Critically, the filter Q-factor should be high and with limited variation across the tuning range in order to ensure stable insertion loss at distinct frequency bands across the passband. Although some Q-factor degradation at the lower frequency end is fundamentally imposed by miniaturisation penalties, this requirement critically implies that penalties associated with reactive load tuning mechanism should be minimised.

The filter requirements for the majority of bands within FR1 can be met by filters with very similar passband bandwidths. Tunable filters should thus maintain an almost constant bandwidth across the tuning range. In terms of the filter implementation, this translates to a coupling matrix that does not significantly change across the various tuning stages. Although tuning mechanisms can be deployed for adjusting both the resonator frequencies as well as the coupling coefficients, this increases the mechanical complexity of the complete assembly that includes not only the filtering structure itself but critically also the reconfiguration mechanism. Filter structures amendable to reconfigurable response that maintain the electrical characteristics across a wide tuning range with a low number of mechanical degrees of freedom are thus advantageous.

The quest for tunable transmit BTS filters

Air-cavity filter technology can conveniently address requirements for high-Q and power handling, although at a cost of elevated volume. Consequently, transmit filters occupy a significant fraction of the radio head volume/surface, which in turn drives the need for miniaturised implementations. A favourable trade-off between performance and size for this class of filters for sub-6 GHz BTS is provided by the coaxial combline topology [1], [3]. Coaxial combline filters that can dynamically adjust their performance has consequently been a topic of intense research over the past years.

A classical way to tune the resonant frequency of coaxial combline resonators involves adjusting the capacitive load at the open end of the resonator, typically combined with tuning the coupling structure [11]. This approach has been adapted for the development of tunable bandpass filters, e.g. [12]-[18]. Since tuning screws reduce the quality factor at the lower edge of the tuning range, the works in [1], [13] proposed an alternative tuning mechanism exploiting rotating loads and hence achieving a 25% improvement of the Q-value in the lower tuning range. Despite the attractive performance characteristics that can be achieved, aforementioned

techniques require independent tuning for each resonator and coupling element. This in turn makes the entire assembly of the filter with an automated tuning mechanism bulky as well as costly and hence unsuitable for compact deployments.

Motived by the needs to reduce costs and the volume of tunable air-cavity combline filters, [12] proposed the integration of coaxial resonators with a microstrip feeding. This approach reduces the complexity of the filtering structure but does not significantly simplify the tuning requirements. In order to simplify the tuning, the works reported in [14], [15], proposed the use of lumped varactor diodes as means to tune the resonators. Similarly, [16] proposed the use of MEMS varactor banks. Despite the attractive features of an integrated tuning mechanism, this approach compromises the Q-factor and the power handling. The work reported in [16] proposed the use of piezo-motors for the tuning of the resonators. This approach, which share similarities with the technique used in [17] for coaxial filters with helical core, can be suitable for narrowband tuning of coaxial combline filters, however in order to cover a broader band additional tuning elements for the coupling structures are required.

A design that accounts for simplified mechanical tuning is reported in [18] where the couplings and frequencies of the resonators are simultaneously controlled by a moveable tuning plate located at the bottom of the assembly. Moving the plate along the two tangential directions allows the resonators and couplings to be tuned at a preselected profile machined on the plate. While this approach reduced the mechanical degrees of freedom, the requirement for translational (rather than rotational) mechanical reconfiguration raises mechanical complexities and potentially also reliability concerns. Moreover this approach led to a limited tuning range of about 18% centred at about 1990 MHz, which is insufficient to cover the range required by emerging 5G New Radio bands.

An alternative approach, developed for applications in satellite communications, employs a common rotating shaft to drive all tuning elements of the coaxial cavity resonators simultaneously is presented in [3]. This approach allows a single rotor to simultaneously tune the frequency of a number of in-line resonators thereby simplifying the mechanical assembly. This work demonstrated tuning of the centre frequency in the range 0.95 GHz to 2.05 GHz. Despite aforementioned advantages, the inter-resonator coupling for this configuration requires the adjustment of additional tuning screws that can be problematic in a BTS scenario. More recently, and in order to address the practical applicability of mechanically tunable filters, [19] presented tunable filter with a constant absolute bandwidth using a single tuning element achieving tuning range of the centre

frequency of 15%. This approach is demonstrated at X-band in an E-plane topology, which is impractically large for applications in L- and C-band.

In this paper we address technical challenges associated with commercial frequency tunable filters for multi-band 4G/5G BTSs. For these systems, and considering the recent and emerging 5G NR standardisation, a main requirement relates to the bandwidth remaining constant across the tuning range of the filter. The solution we propose enables compact and high performance frequency adjustable cavity filters based on a mechanical solution with stepper motors (an individual motor per resonator for asynchronous tuning of the center frequency of each resonator) bringing unique advantages that include; compact size (as low as 26.6° electrical length at 737.5 MHz, and as low as 33.9° electrical length; calculated for a resonator of 30 mm in height); constant bandwidth across the frequency range (varies from 2.66 % to 2.89 %); reduced mechanical complexity (tuning is only required to adjust the center frequency of each resonator and not the coupling elements); wide tuning range, and; high-performance across the wide tuning range including low insertion loss (measured in the range 0.66-0.98 dB for 6-resonator filters in Aluminum), excellent return loss (measured return loss better than -18 dB) as well as suitability for advanced filter responses with multiple transmission zeroes generated at both sides of the passbands.

Operating Principle

In order to achieve wide tuning range the following two conditions need to be met. On one hand, the individual resonators should simultaneously tune to the desired band. On the other hand, the coupling between input/output ports as well as between the resonators should adhere to the coupling matrix requirements across different center frequencies. Adjusting the resonant frequency of a coaxial combline resonator can be achieved by adjusting the reactive loading at its open end. However this typically affects the field distribution in the surrounding region and consequently the realised coupling coefficients.

A technique to produce a compact coaxial combline resonators is described in [20], [21]. It entails two coaxial lines emanating from both sides of a cavity that are interlaced in the middle producing increased capacitive loading (Figure 2). This technique achieves very good trade-offs between miniaturisation, tuning range and Q-factor. Critically, the resonator layout effectively provides a shields for the fields associated with the reactive loading within an enclosed cavity; consequently the field distribution in the area surrounding the resonator, which defines the inter-resonator coupling, does not significantly change as the operating frequency is tuned and hence the variation of the coupling coefficient at different resonant frequencies are negligible.

Figure *2* illustrates the operating principle of the reconfigurable resonators. The layout of the resonator is shown in Figure *2a*, while Figure *2b* shows a pair of resonators coupled through an inductive window. By means of adjusting the capacitive load tuner, the resonant frequency can be adjusted. Figure *2c* shows the tuning range of an individual resonator as a function of the mechanical movement of the tuner. As shown the length of the tuner delivers an almost linear adjustment of the operating frequency of approximately 15 MHz/mm. The achieved frequency tuning range extends outside the usable tuning range for our application. The Q-factor of the resonator as it is tuned between the two extreme frequency positions is plotted in Figure *2d*. An almost linear dependence of the Q-factor vs the frequency is demonstrated. In, particular, and limiting the frequency range within our required application range (737.5 MHz – 942.5 MHz), for a frequency change of ~26 %, the Q-factor is changed by ~25.8 %. The Q-factor does not significantly degrade due to the mechanical contact of the moving parts, but only reflects the smaller electrical length for a fixed physical size and thus, it is a design parameter. Thus, the size of the tunable filter is mostly designed based on the performance required at the minimum frequency tunable state.

Another advantageous characteristic for this topology is summarised in Figure *2e* and Figure *2f*. In particular, Figure *2e* plots the group delay at the input and output port for different operating frequencies of the resonator. The typical inductive coupling to a post connected to a coaxial port is considered, as described in [20], [21]. As shown, the group delay is fairly stable across the operating frequencies of the resonator, which allows maintaining good impedance matching across the entire tuning range. Similarly, Figure *2f* shows the variation of the coupling coefficient (normalised to its maximum value) for a pair of synchronously coupled resonators tuned at different frequencies. Different curves correspond to different values for the width of the inductive window, marked as slotW in the legend, normalized to the maximum width that corresponds to the cavity width.

There are two main observations to be made from this plot. On one hand the variation across of the coupling coefficient across the entire frequency range is less than 10%. On the other hand, the variation of the normalised coupling coefficient is effectively independent from the width of the coupling window. Since the latter defines the absolute value of the coupling, the combined observations from Figure *2f* indicate that as the filter is tuned to a different center frequency, the individual inter-resonator couplings vary only within 10% of their value and, perhaps more critically, this fractional variation is fixed across all inter-resonator couplings of the filter. The above observation implies that a simple and efficient tuning can be achieved with the number of

mechanical adjustments limited only to those required in order adjust the operating frequency of the resonators.

Performance Characteristics

In this section we present the performance characteristics of the proposed filters by means of two implemented examples. By means of full wave simulations and experimental results, we illustrate the tuning range that can be achieved, the return and insertion loss characteristics, the implementation of cross-coupling architectures for introducing TZs, and finally, review the integration of the mechanics into the filter. A challenging aspect relating to the practical application of frequency adjustable filters relates to the return loss remaining stable across with the operating range, such that the filter is well matched at all operational stages. Our goal is that the return loss remains acceptable at all frequencies, here targeting values better than 18 dB.

A stepper motor is attached to each individual resonator to provide a linear movement of the resonator tuner in and out of the resonator cavity. The number of steps for each motor is managed by a control unit, which consists of stepper motor drivers and a microcontroller where the control software runs. The steps are translated to an equivalent mechanical penetration of the tuner into the resonator cavity. The selected thread is chosen such that a full 360° turn of the stepper motor is translated to a mechanical movement of 0.5 mm. With a 20 step per turn resolution chosen for the stepper motor, the mechanical resolution per step is 25 um. As will also be demonstrated experimentally, this provides good repeatability when considering the accuracy of stepper motors in delivering the same number of steps. Given that the tuner provides an approximate 15 MHz / mm (*Figure* 1d), the above further indicate an average frequency resolution of about 375 KHz. If required, this can further be adjusted by controlling the thread of the tuner.

Figure *3*a shows the CAD model of a 6 pole filter with the integrated mechanics of the stepper motors. The number of the stepper motors is equal to the number of resonators, i.e. there is no requirement for additional mechanics to control the inter-resonator coupling and the input/output coupling. This in turn simplifies the mechanics and the electronic control systems, thereby minimizing volume, complexity and cost. Moreover, mechanical simplicity minimizes the components that can lead to failure. The filter design has targeted the downlink 5G NR 3GPP frequency bands below 1 GHz, where the low frequencies give rise to the most stringent requirements in terms of volume and mass.

The simulated response of the frequency adjustable filter at three distinct frequency bands including two bands on either end of this range (band n12: f_0=737.5 MHz and band n8: f_0=942.5 MHz) as well as a center band

(band n5: f_0=881.5 MHz) [21] is shown in Figure *4*a. It is noted that additional margins of the order of 5 MHz are allowed to address manufacturing tolerances, thermal and other distortions; together with the capability to tune each individual resonator along a wide frequency range, this strategy allows to effectively mitigate the impact of manufacturing tolerances. Exclusive of these margins, the simulations indicate a tuning range of 205 MHz, between 737.5 MHz and 942.5 MHz, representing a fractional value of 24.4%. The return loss is always maintained better than -18.5 dB. As discussed, the stable input/output coupling and inter-resonator coupling allows good matching of the filter at the different frequencies.

Figure *4* shows a 6-pole filter in a folded configuration. A symmetric transmission zero is generated in this folded configuration to improve the out-of-band performance of the filter. The simulated response is shown in Figure *4* where the filter is tuned along the same frequency bands. It is shown that the transmission zeroes follow similar trends in the frequency as the center frequency of the filter. This is attributed to the stable coupling coefficient values achieved for the cross-coupled resonators and, significantly, enables introducing TZs that follow the frequency variation of the passband. In this example, this property allows maintaining the same sharp near out of band rejection across the tuning range of the filter and thereby meet the requirements of the most demanding applications. It is noted that in the presented designs the location of the TZs serves to achieve the required isolation between the Tx and Rx filters. The demonstrated stability of the TZs location over the 25 % tuning range is a significant advance of the state-of-the-art. As the tuning range might increase further, then problems due to frequency dispersion of the couplings, might arise. The capability to produce transfer functions with selected TZs that maintain the desired location with respect to the passband across different operating frequencies is valid for other filter topologies and has been confirmed by another design example (not shown for brevity) demonstrating the ability to introduce two TZs on the upper side only. For completeness, Figure *5* shows the simulated response of the filter in Figure *4* in two cases, a case without transmission zeroes and the case with the transmission zeroes.

Figure 6 shows photographs of two filter prototypes that have been manufactured and tested. The photographs show the integration of the stepper motors with the filter cavity. The measurement results reported in this section have been conducted with an Agilent N5241A PNA-X network analyser. Figure 7 shows the measurement results of the 6-pole frequency adjustable filters. The filters were tested at the two extreme bands as well as the mid-frequency band. As per simulations, the measured tuning range is 205 MHz representing a range of 24.4%.

A common problem in the implementation of frequency adjustable filters is that the insertion loss introduced by the mechanics of the tuning mechanism usually varies significantly with the frequency. This in turn has implications in the physical layer management. In order to illustrate the insertion loss variation, Figure 7 shows the insertion loss of the 3 measured bands as compared to the simulated cases. The measured insertion loss varies between 0.67 dB to 0.98 dB (in Aluminum), which indicates that the difference in insertion loss between the two extreme frequencies is 0.32 dB (in measurement for Aluminum) whereas in simulation the equivalent value is -0.16 dB. Once the filters were silver-plated, the measured insertion loss across the two extreme frequencies varies between 0.54 dB to 0.75 dB, indicating a difference of 0.21 dB that approaches the simulated value. Considering that the simulated results involve a static structure where all metal contacts are perfect (no moving parts), the above measurement result proves that this technology allows maintaining the high performance of filters under the frequency range of adjustment.

It is noted that increased insertion loss at the lower frequency bands is fundamentally anticipated for two reasons. Firstly, at a lower frequency a fixed passband is of narrower fractional value, which in turn is a known factor for higher insertion loss. Moreover, at a lower frequency the resonators are electrically smaller and the higher level of miniaturisation is another known factor for higher insertion loss. In light of the above, an advantageous characteristic of the proposed solution is that insertion loss penalties associated with frequency tuning are minimized and high Q factor values (in the range 2900-2300) are maintained across the entire tuning range. Consequently, the insertion loss of the filters in the worst frequency scenario remains very low.

Repeatability Tests: In order to validate the stability and repeatability of the filter response, an experimental campaign entailing repetitive measurements has been conducted. Figure 8 shows results of the measurements that involves a continuous testing of the filters. The adjustable filter is pre-tuned for 7 frequency bands and the values of the positions of the tuning pistons are stored. The filter is retuned to each of these bands sequentially for 200 times in a total of 1400 measurements. The measurement campaign lasted for 5.5 hours.

Figure 8a show the measured return loss and transmission of the filter, respectively, where all the 1400 measurements are superimposed. These two graphs demonstrate the stability and repeatability of the filter response. Figure 8b-e show a closer look into the measured results of Figure 8a for four individual frequency bands, the two lower and two higher frequency bands. As shown, the frequency response is well reproduced. Some higher variation at the lower frequency end can be understood in light of the steeper slope of the curve in Figure 1c, that indicates elevated frequency sensitivity with the tuner penetration towards lower frequencies.

Figure *9* shows the probability distribution function of the insertion loss for all the 7 measured frequency bands as obtained from this test campaign. As shown, higher frequency bands are associated with reduced values for both the average insertion loss as well its variance. These observations are consistent with the discussions above. Finally, Figure *10* shows the measured out-of-band response of the frequency adjustable filter operating at all bands indicating good repeatability.

Environmental Tests

A set of environmental tests have been conducted in order to qualify the filter technology against specification requirements of commercial BTS filters. These include temperature cycling tests, vibration tests as well as power handling tests. The temperature tests include a high temperature test and temperature cycling tests. Some selected measured results for the three bands (n12, n5, n8) at three different temperatures are shown in Figure *11* (the filter prototype measured is that of Figure *4* after silver-plating). As shown, the temperature variation and associated thermoelastic distortions lead to frequency drifts of the order of 1 MHz. Significantly, the integrated tuning mechanism allows to dynamically correct for any frequency drifts associated with temperature variations.

Vibration tests include tests per physical axis; sinusoidal, random and shock vibration tests. Tests were done according to ETSI standard on environmental conditions and environmental tests for telecommunications equipment and in particular the specification of environmental tests for stationary use at non-weather protected locations [22]. During all tests the filter were functionally measured with Agilent E5071C ENA. All the measured filters have passed the tests.

Finally, power handling tests include tests for average and peak RF power handling. A set of prototype filters has been measured for functionality, prior to the tests, during the tests and afterwards. Visual inspection of the filters was also done after the peak power measurements. The adjustable filters have passed all the tests with measured peak power exceeding 2200 W.

The combined repeatability test campaign together with the environmental tests indicate high reliability and useable lifetime for the proposed filters.

Conclusions

We have proposed a new class of compact tunable coaxial filters that are capable of adjusting the centre frequency of a fixed passband and adjacent transmission zeros across a wide frequency range. The proposed

filters maintain mechanical simplicity and high performance indicated by favourable insertion loss and return loss measurements. Two example designs have been implemented and integrated with stepper motors. Repeatability and environmental test campaigns have indicated highly robust devices, which are suitable for deployment in agile multiband cellular BTSs supporting 5G NR bands. Replicating the fractional tunability achieved here for sub-1 GHz bands will enable covering the vast majority of sub-6 GHz 4G and 5G bands with 3 filters. This would significantly reduce the variance of RF products required to cover associated systems with significant benefits for time-to-market, cost and agility. The proposed filters may also find applications in other terrestrial and satellite communication systems.

References:

[1] R. J. Cameron, C. M. Kudsia, and R. R. Mansour, "Tunable Filters," in *Microwave Filters for Communication Systems: Fundamentals, Design, and Applications*, Hoboken, NJ, USA: Wiley 2018.

[2] R. R. Mansour, F. Huang, S. Fouladi, W. D. Yan and M. Nasr, "High-Q Tunable Filters: Challenges and Potential," *IEEE Microw. Magazine*, vol. 15, no. 5, pp. 70-82, Jul.-Aug. 2014.

[3] M. Yu, B. Yassini, B. Keats and Y. Wang, "The Sound the Air Makes: High-Performance Tunable Filters Based on Air-Cavity Resonators," *IEEE Microw. Magazine*, vol. 15, no. 5, pp. 83-93, Jul.-Aug. 2014.

[4] D. Peroulis, E. Naglich, M. Sinani and M. Hickle, "Tuned to Resonance: Transfer-Function-Adaptive Filters in Evanescent-Mode Cavity-Resonator Technology," IEEE Microw. Magazine, vol. 15, no. 5, pp. 55-69, Jul.-Aug. 2014.

[5] J. R. Bogdanovic, G. M. Donic, M. D. Sarenac and S. M. Milosevic, "Tunable UHF TV channel power filter optimization," in *12th Intern. Conf. on Microw. & Radar, MIKON-98*, (Conference Proceedings IEEE Cat. No.98EX195), Krakow, Poland, 1998, pp. 18-22 vol.1.

[6] K. Pence and G. Rochford, "Multiple Band and Multiple Frequency Dielectric Resonators Tunable Filters for Base Stations," in *38th Europ. Microw. Conf.*, Amsterdam, The Nether. 2008, pp. 488-491.

[7] D. Psychogiou, R. Gómez-García and D. Peroulis, "Recent advances in reconfigurable microwave filter design," in *IEEE 17th Annual Wirel. & Microw. Tech. Conf. (WAMICON)*, Clearwater, FL, 2016, pp. 1-6.

[8] Acar, Öncel, Tom K. Johansen, and Vitaliy Zhurbenko. "A high-power low-loss continuously tunable bandpass filter with transversely biased ferrite-loaded coaxial resonators." *IEEE Trans. Microw. Theory & Techn.* Vol. 63, no. 10, pp. 3425-3432, Oct. 2015.

[9] A. Mahmoud, and D. Peroulis. "High-Q Tunable Evanescent-Mode Cavity SIW Resonators and Filters With Contactless Tuners," *IEEE Trans. Microw. Theory & Techn.* Vol. 67, no. 9, pp. 3661-3672, Sep. 2019.

[10] 3GPP Specification series: Base Station (BS) radio transmission and reception (3GPP TS 38.104 version 15.2.0 Release 15) https://www.etsi.org/deliver/etsi_ts/138100_138199/138104/15.02.00_60/ts_138104v150200p.pdf

[11] C. Kwak, M. Uhm and I. Yom, "Feasibility study on combline filter for tunable filters," in *Asia-Pacific Microw. Conf. (APMC)*, Seoul, Kor. 2013, pp. 927-929.

[12] S. Kurudere and V. B. Erturk, "Novel Microstrip Fed Mechanically Tunable Combline Cavity Filter," *IEEE Microw. and Wirel. Comp. Lett.*, vol. 23, no. 11, pp. 578-580, Nov. 2013.

[13] M. A. Iskander, M. Nasresfahani and R. R. Mansour, "A constant-Q tunable combline bandpass filter using angular tuning technique," in *44th Europ. Microw. Conf.*, Rome, It. 2014, pp. 1103-1106.

[14] A. Anand and X. Liu, "Reconfigurable Planar Capacitive Coupling in Substrate-Integrated Coaxial-Cavity Filters," *IEEE Trans. on Microw. Theory & Techn.*, vol. 64, no. 8, pp. 2548-2560, Aug. 2016.

[15] Xu, Jin-Xu, Lian Yang, Yang Yang, and Xiu Yin Zhang. "High-Q-Factor Tunable Bandpass Filter With Constant Absolute Bandwidth and Wide Tuning Range Based on Coaxial Resonators," *IEEE Trans. Microw. Theory & Techn.*, Vol 67, no. 10, pp. 4186-4195, Oct. 2019.

[16] S. Fouladi, F. Huang, W. D. Yan and R. R. Mansour, "High-Q Narrowband Tunable Combline Bandpass Filters Using MEMS Capacitor Banks and Piezomotors," *IEEE Trans. Microw. Theory & Techn.*, vol. 61, no. 1, pp. 393-402, Jan. 2013.

[17] D. Psychogiou and D. Peroulis, "Tunable VHF Miniaturized Helical Filters," *IEEE Trans. Microw. Theory & Techn.*, vol. 62, no. 2, pp. 282-289, Feb. 2014.

[18] M. Hoft, A. Kronberger, O. Bartz, "Tunable bandpass filters for multi-standard applications," in *German Microw. conf.*, Germ. 2008, pp. 1-4.

[19] Basavarajappa, Gowrish, and Raafat R. Mansour. "Design Methodology of a Tunable Waveguide Filter With a Constant Absolute Bandwidth Using a Single Tuning Element," *IEEE Trans. Microw. Theory & Techn.* Vol. 66, no. 12 (2018): 5632-5639.

[20] E. Doumanis, S. Bulja, D. Kozlov, "Compact coaxial filters for BTS applications," *IEEE Microw. & Wirel. Compon. Lett.*, Vol. 27 (12), pp. 1077-1079, Dec. 2017.

[21] C. Hallet, J.-F. Favennec, E. Rius, J. Benedicto, L. Carpentier, and D. Pacaud, "Optimization of an Air Filled Compact Re-Entrant Coaxial Resonator for a C-Band Bandpass Filter," IEEE Access 6 (2018): 54117-54125.

[22] ETSI EN 300 019-2-4 V2.4.6 (2018-03) Environmental Engineering (EE); Environmental conditions and environmental tests for telecommunications equipment; Part 2-4: Specification of environmental tests; Stationary use at non-weather protected locations.

(a)
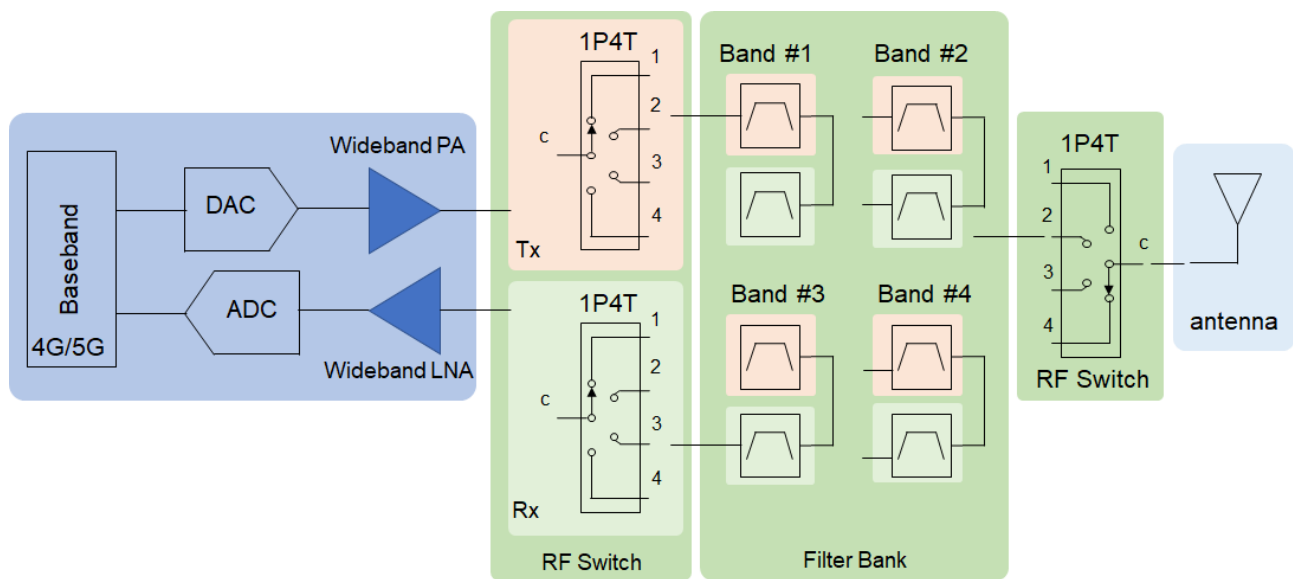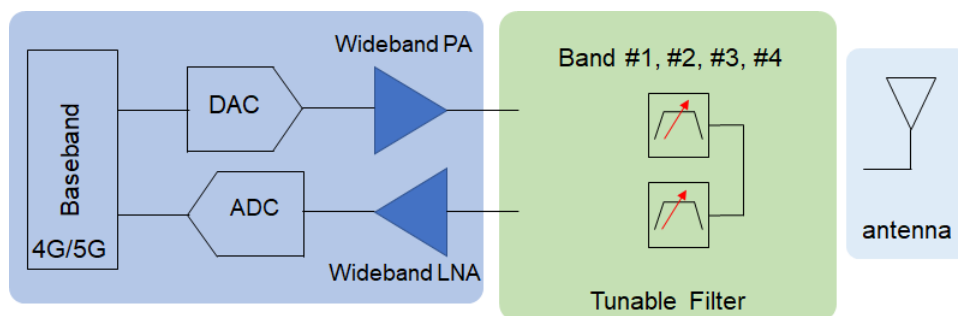
Figure 1: Simplified generic system block diagram for the transmit chain of an agile multiband Base Transceiver station, a) implementation with a filter bank; b) implementation with tunable filters.

(a)

(b)

(c)

(d)

(e)

(f)
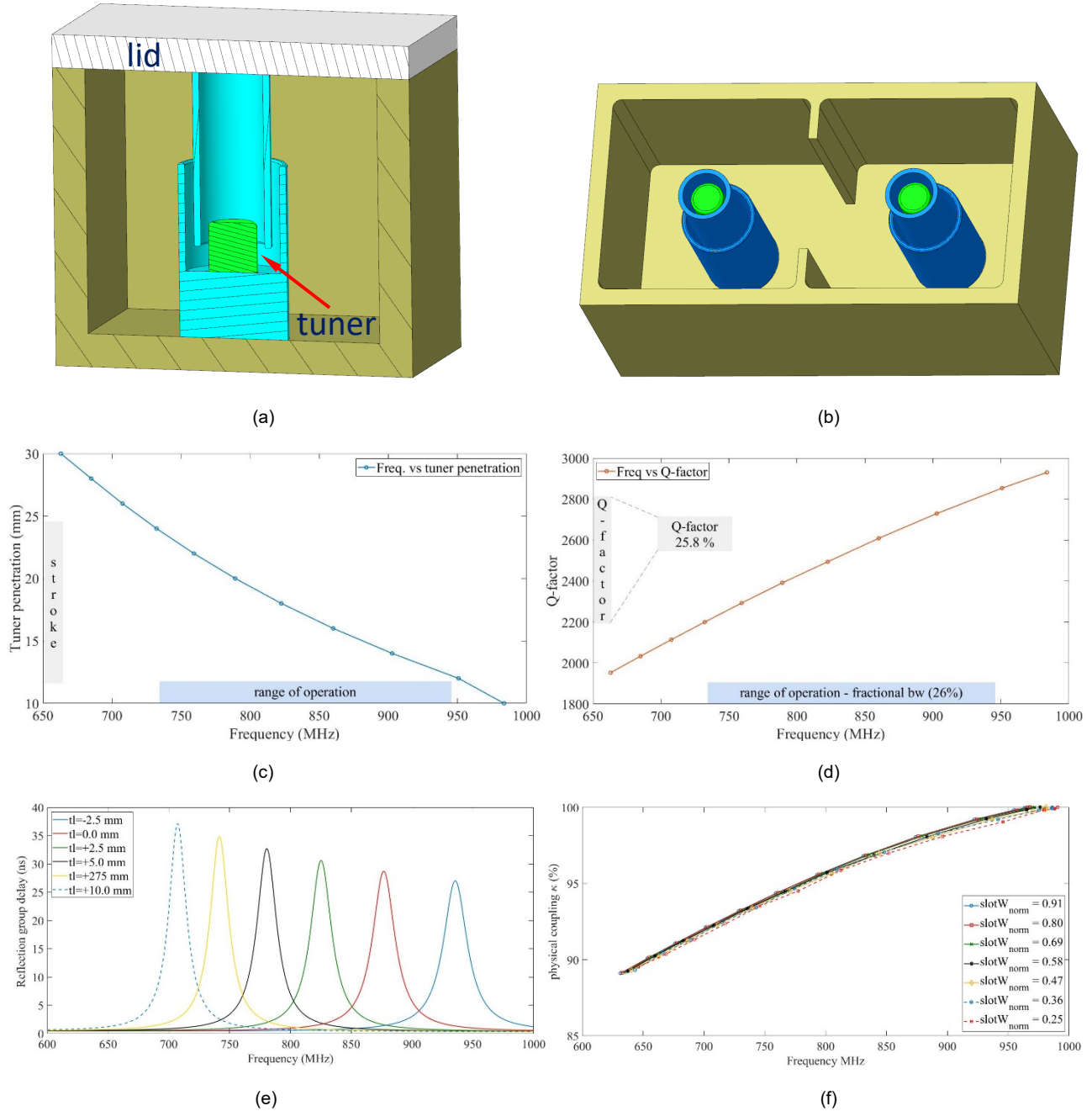
Figure 2: Operating principle: a) CAD model of a single resonator, b) CAD model of a resonator pair coupled with an inductive slot. c) relationship between the resonant frequency and the length of the tuner indicating a good resolution of average of about 15 MHz per 1mm, d) simulated Q-factor at different tuner lengths e) simulated input port reflection group delay of a single resonator at the excitation port for different operating frequencies; as shown the group delay varies from 27 to 37.1 ns representing 31.5 % variation within the frequency band of interest f) simulated coupling of a pair of resonators as a function of center frequency for a range of different width coupling slots (normalized to the maximum width).
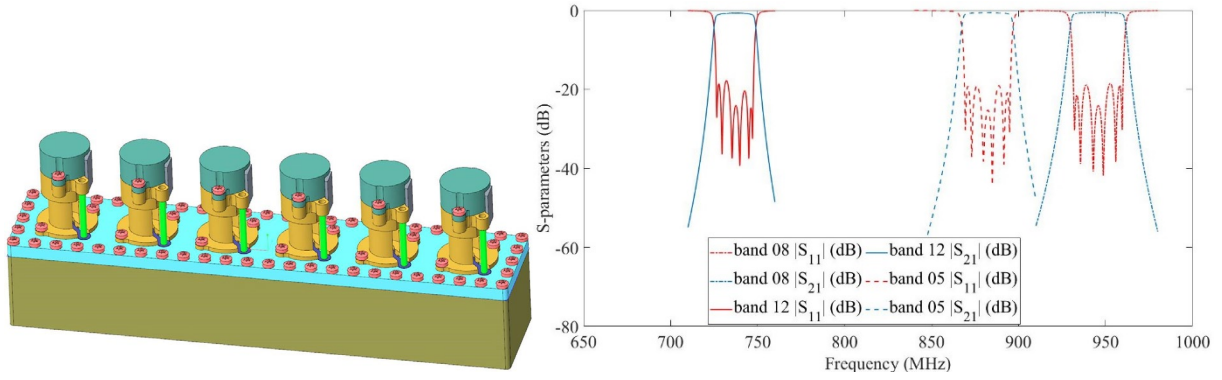
Figure 3: CAD model of a 6-pole filter prototype. The models show the integration of stepper motors to the cavity of the filters. Simulated results of frequency adjustable filters The filter is tuned at 3 distinct bands, band n5-f_0=881.5 MHz, band n12 – f_0=737.5 MHz, and band n8- f_0=942.5 MHz. The figure shows the wideband response of these three filter configurations.
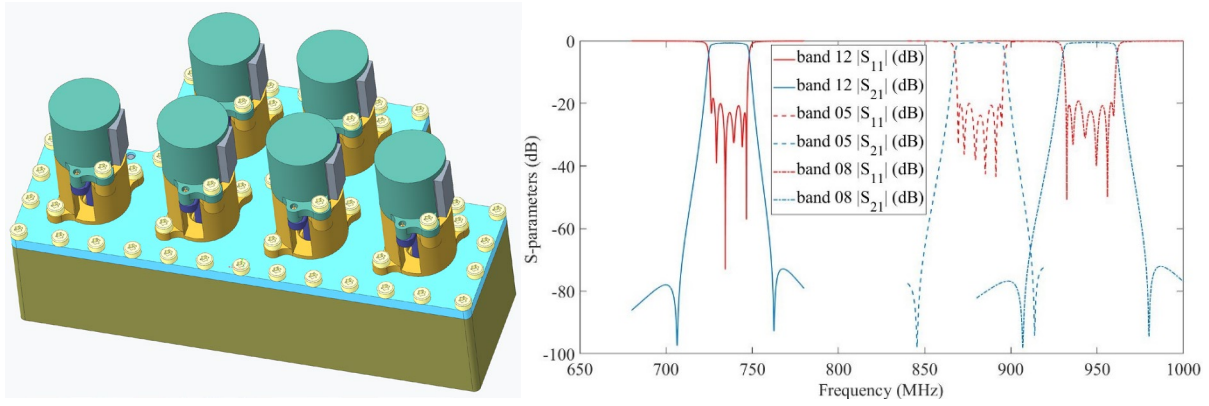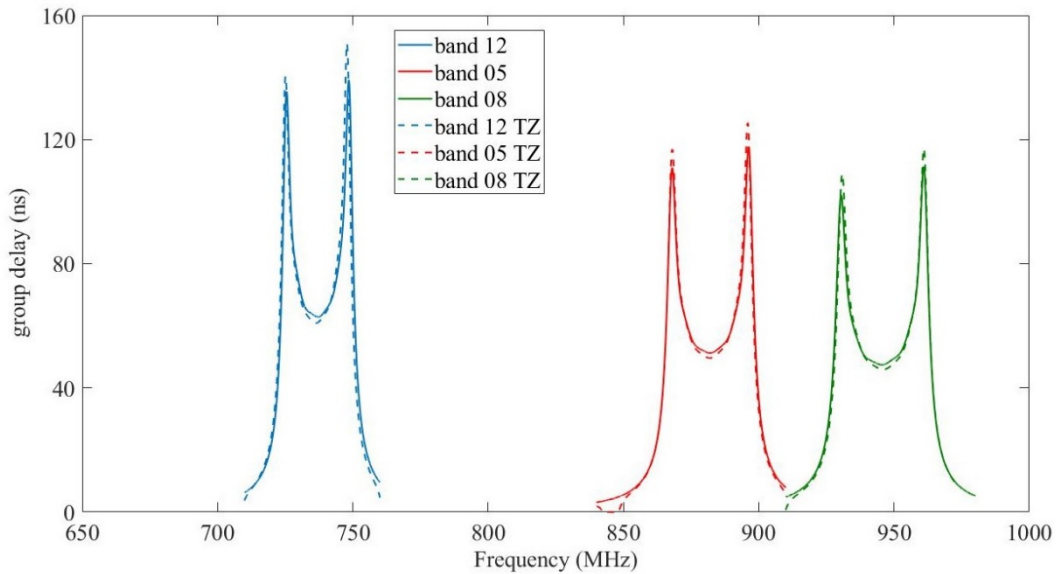

Figure 4: CAD model of 6-pole filter prototype. The employed resonator is 34x34x30 mm^3. The model shows the integration of stepper motors to the cavity of the filter. Simulated results of frequency adjustable filters with TZs. The filter is tuned at 3 distinct bands, band n5-f_0=881.5 MHz, band n12 – f_0=737.5 MHz, and band n8- f_0=942.5 MHz. The figure shows the wideband response of these three filter configurations.

Figure 5: Simulated group delay (ns) of the filter of Figure 4 at 3 frequency bands for two simulated cases, with no TZs and with TZs.
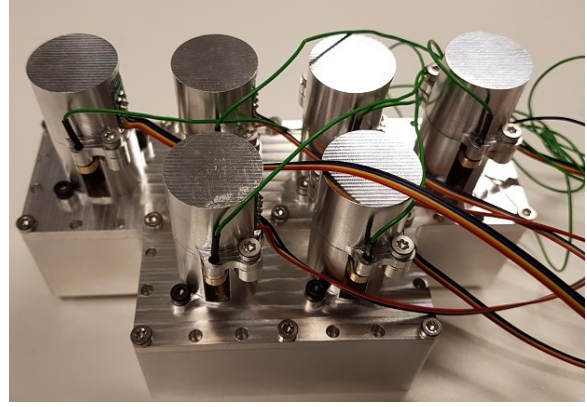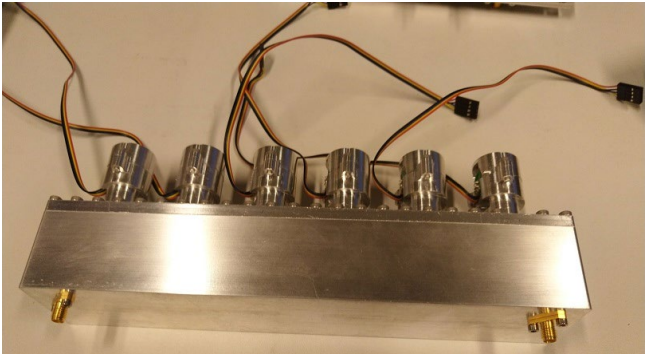
Figure 6: Photographs of two 6-pole filter prototypes of Figure 3 and Figure 4. The photographs show the integration of stepper motors to the cavity of the filters. The filters are made of Aluminum. In the first prototype the tuners are made of aluminum whereas in the second prototype are made of brass.
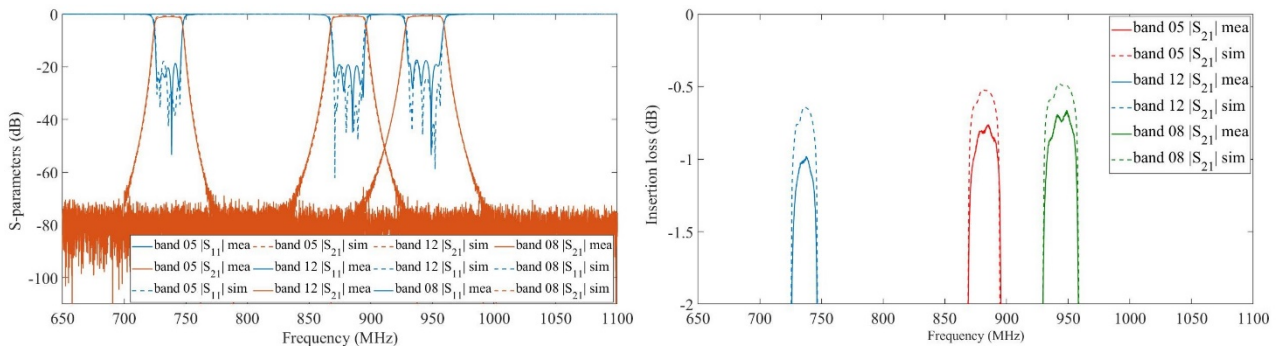

Figure 7: Measured results of frequency adjustable filter of Figure 3 – Simulated results superimposed for comparison a) Measured results of the frequency adjustable filter. The filter is pre-tuned at 3 distinct bands, band n5-f0=881.5 MHz, band n12 – f0=737.5 MHz, and band n8- f0=942.5 MHz. The figure shows the wideband response of these three filter configurations. b) Measured insertion loss of the frequency adjustable filter.
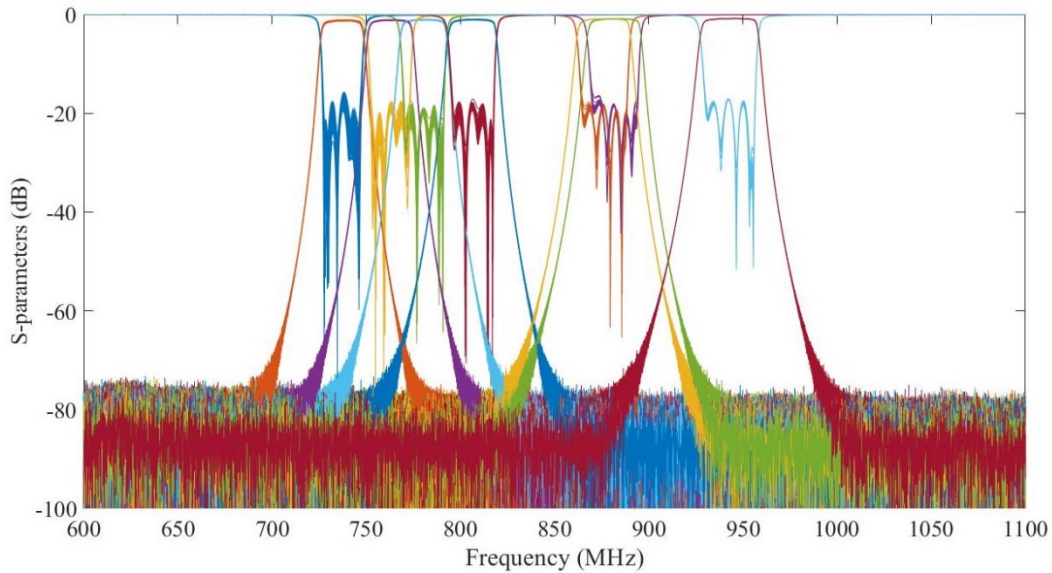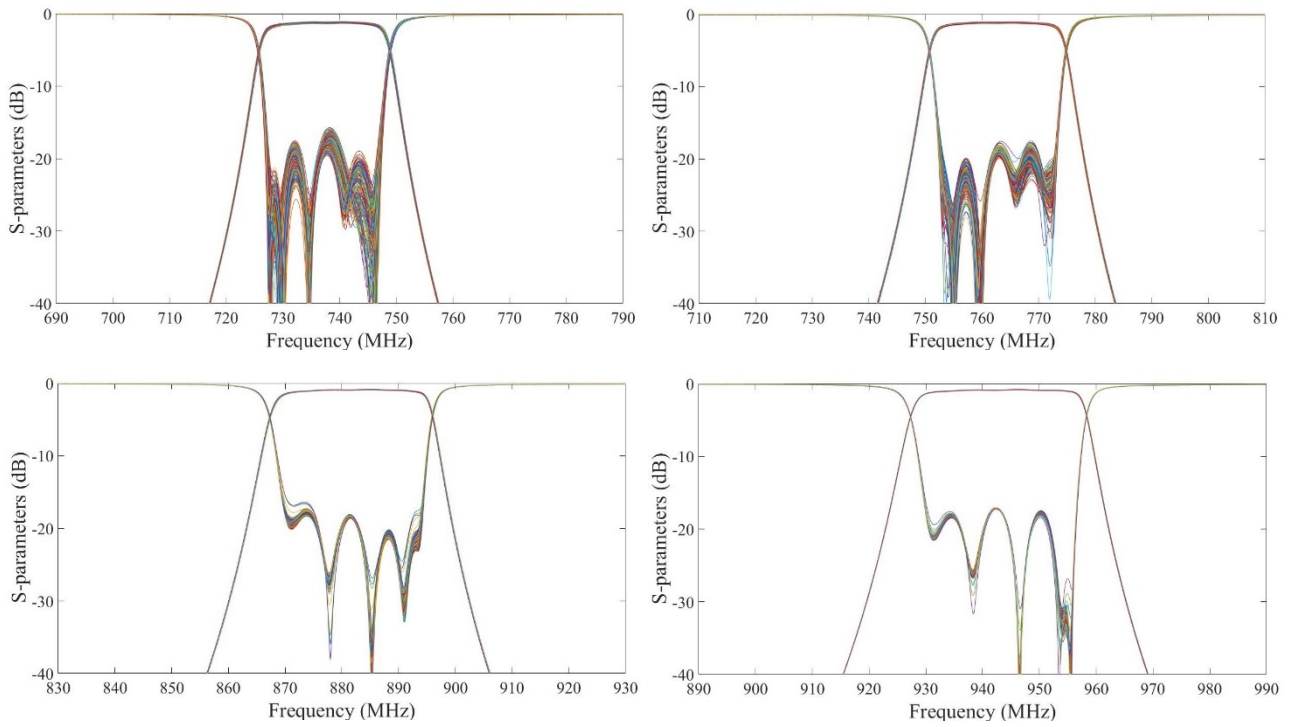
Figure 8: Repetitive experimental campaign of the filter prototype of Figure 3: The filter is pre-tuned for 7 frequency bands. The filter is tuned at the first band and then measured. Then, the filter is tuned at the second band and the re-measured. A matlab script controls the stepper motors and the VNA. This process is done for 1400 times with a total measurements time of 5.5 hours. The response of each filter is superimposed for 200 times for each band, a total of 1400 measurements are plotted. The lowest two frequency bands and the highest two bands are also shown. Each graph shows the 200 measurement results superimposed.
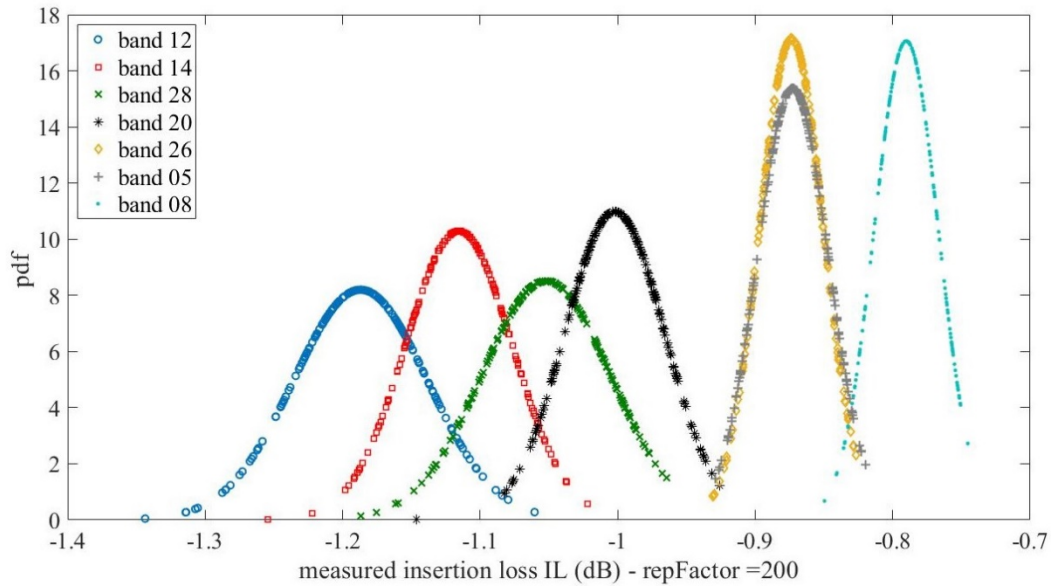

Figure 9: Repetitive experimental campaign of the filter prototype – processed results: The reported results shown in Figure 8 are repeated here for a closer look at the insertion loss data. The figure plots the probability distribution function (normal distribution) of the measured insertion loss data for all measurements (against the frequency index for all the 7 bands).
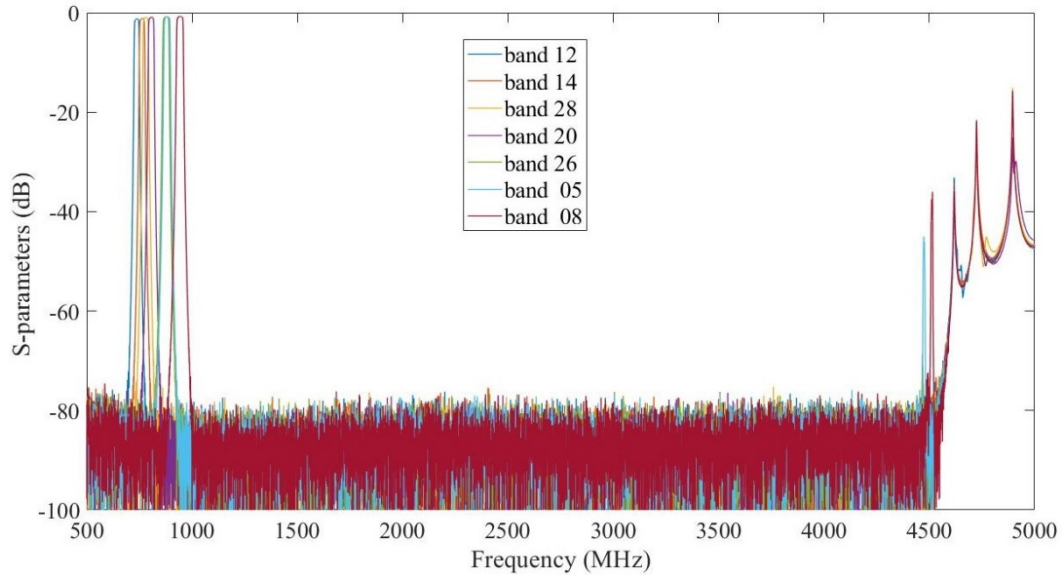
Figure 10: Out-of-band measured results of frequency adjustable filters to demonstrate the harmonic output of the filters. The filter is pre-tuned at 7 distinct bands. The figure shows the wideband transmission response of these seven filter configurations.
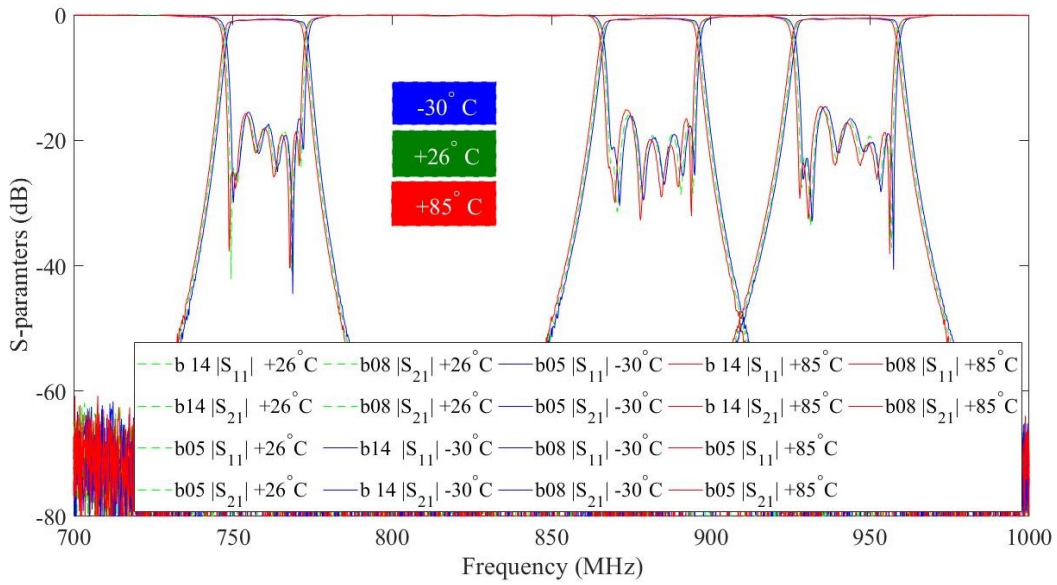

Figure 11: Thermal test campaign of the filter prototype of Figure 4 (silver-plated) across three different bands at three frequencies. Blue curve represents the -30° C case, the green curve represents room temperature and the red curve represents the +85° C.